

A Direct-write Method for Preparing Bimetal Sulfide/Graphene Composite as a Free-standing Electrode for High-performance Microsupercapacitors

Hao Liu, Xiaojuan Liu, Fengying Dong and Xinzhi Sun*

College of Chemistry and Pharmaceutical Sciences, Qingdao Agricultural University,

Qingdao 266109, China

*Corresponding author: Tel/Fax: 86-532-58957855;

E-mail: xzsun@qau.edu.cn

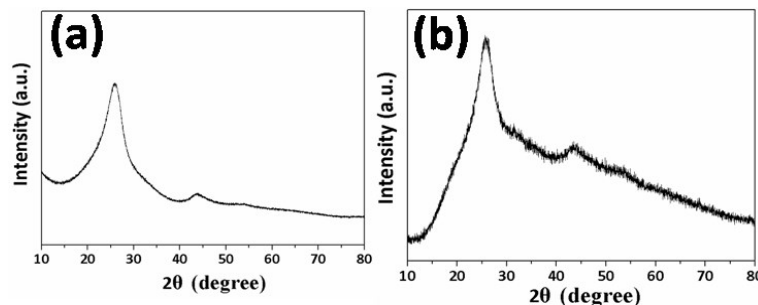


Fig. S1 XRD patterns of the carbon cloth (a) and Ni-Co precursor/C.C (b)

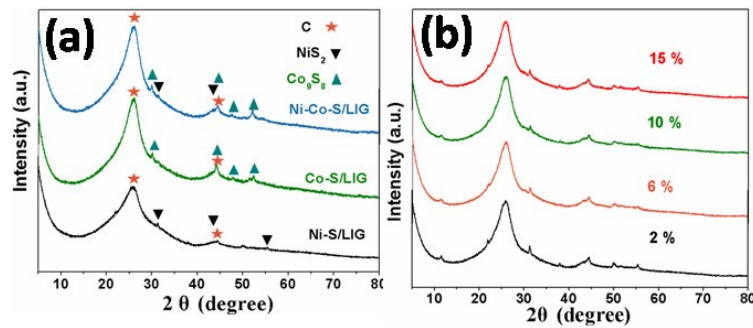


Fig. S2 XRD patterns of (a) Ni-Co-S/LIG, Co-S/LIG , Ni-S/LIG and (b) the different amounts of cobalt in Ni-Co-S/LIG

Table S1 D, G and 2D bands and the ratio of I_G/I_D of LIG, starch-LIG and Ni-Co-S/LIG

	LIG	Starch-LIG	Ni-Co-S/LIG
I_G/I_D (Height)	1.05	0.99	1.34
D-band	1359	1356	1368
G-band	1595	1592	1583
2D-band	2793	2738	2749

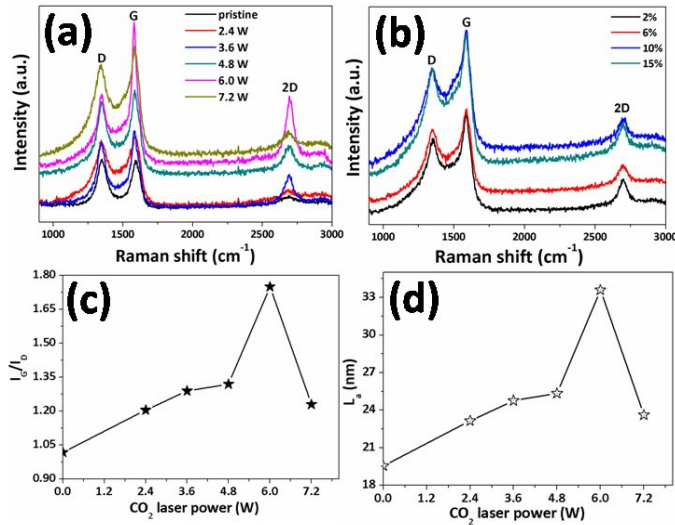


Fig. S3 Raman spectra of LIG obtained with different laser powers (a) and Ni-Co-S/LIG with different Co content (b),

Table S2 D, G and 2D bands and the ratio of I_G/I_D of Ni-Co-S/LIG with the different Co content

	2%	6%	10%	15%
I_D/I_G (Height)	1.33	1.34	1.35	1.30
D-band	1381	1368	1373	1375
G-band	1588	1583	1580	1582
2D-band	2728	2749	2740	2744

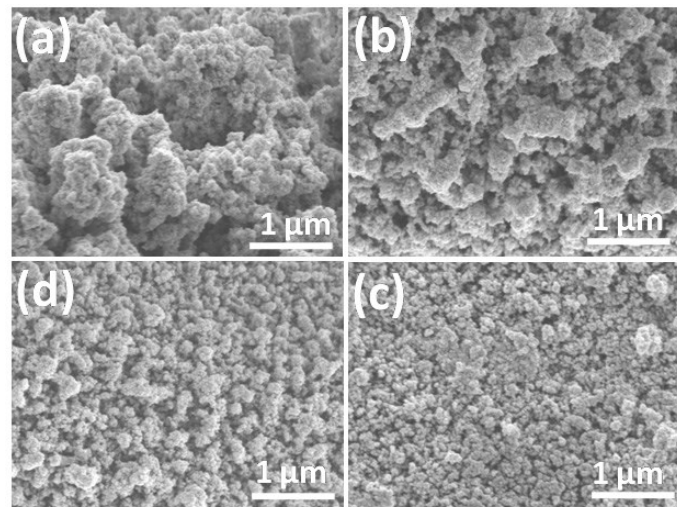


Fig. S4 SEM images of Ni-Co-S/LIG with different Co content

(a) 2%, (b) 6%, (c) 10%, (d) 15%

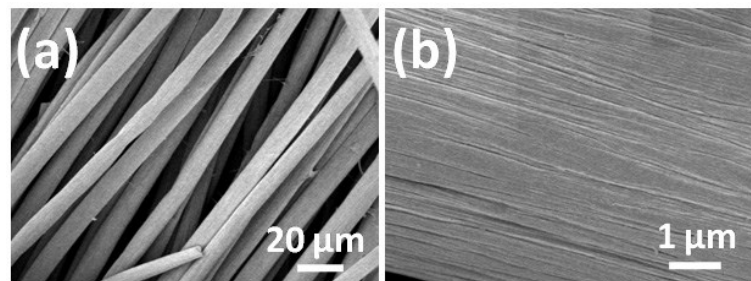


Fig. S5 SEM images of carbon cloth without laser scribbling

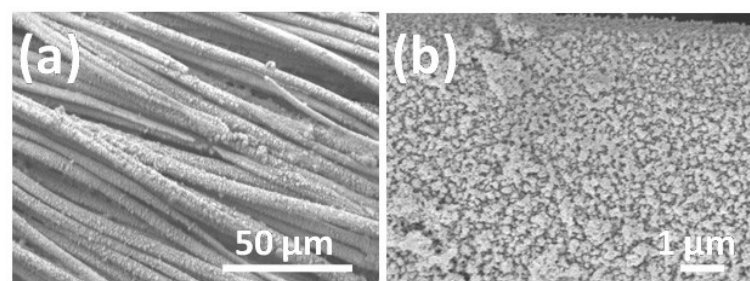


Fig. S6 SEM images of Co-S/LIG

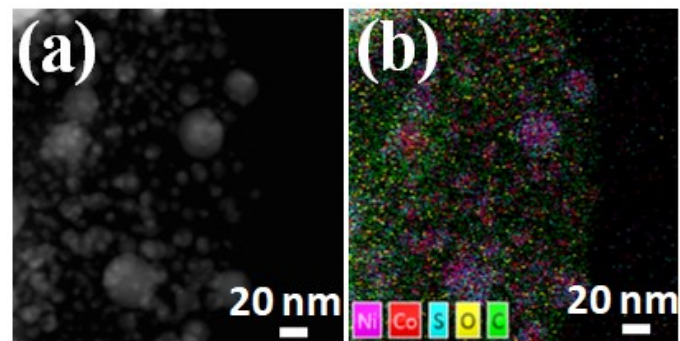


Fig. S7 EDS layered images of Ni-Co-S/LIG

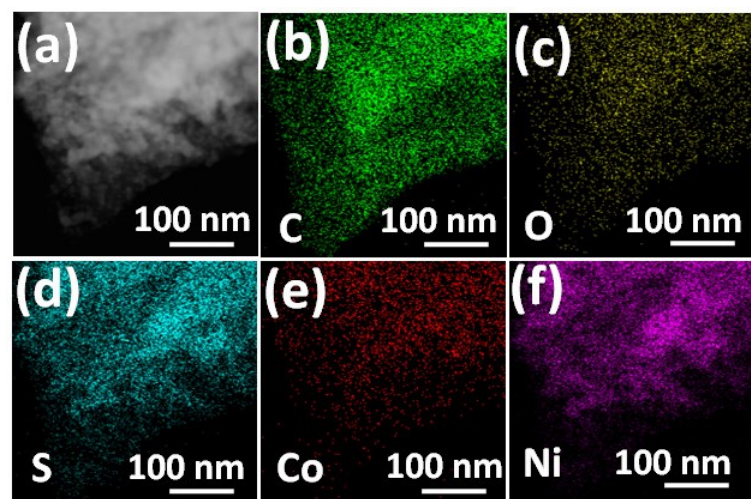


Fig. S8 The corresponding element distribution mapping of carbon (b), oxygen (c), sulfur (d), nickel (e), cobalt (f), respectively. Inset (a) is the TEM image of Ni–Co–S/LIG

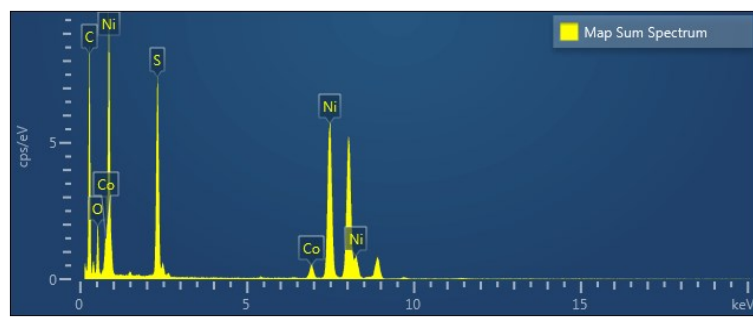


Fig. S9 EDS spectrum of Ni-Co-S/LIG (the corresponding TEM shown in Fig. S7)

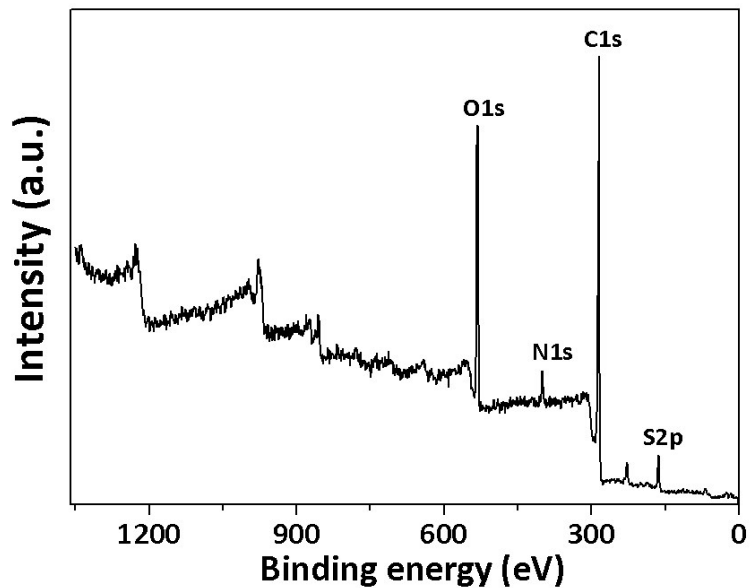


Fig. S10 The survey XPS spectrum of Ni-Co-S/LIG:

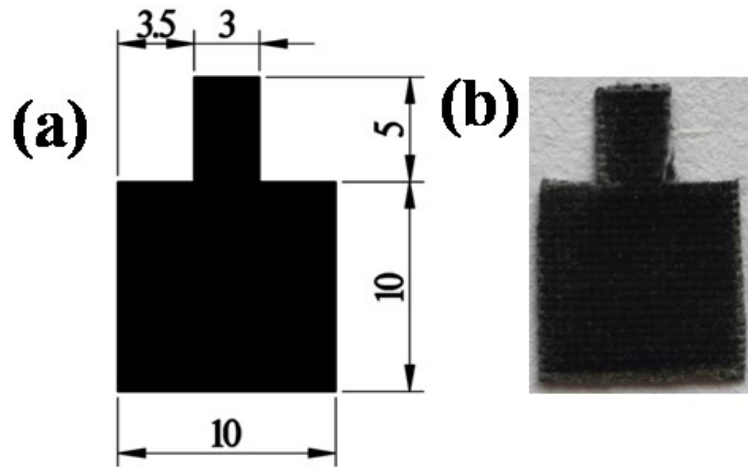


Fig. S11 The dimension of the Ni-Co-S/LIG electrode in plane (a) and the real sample (b)

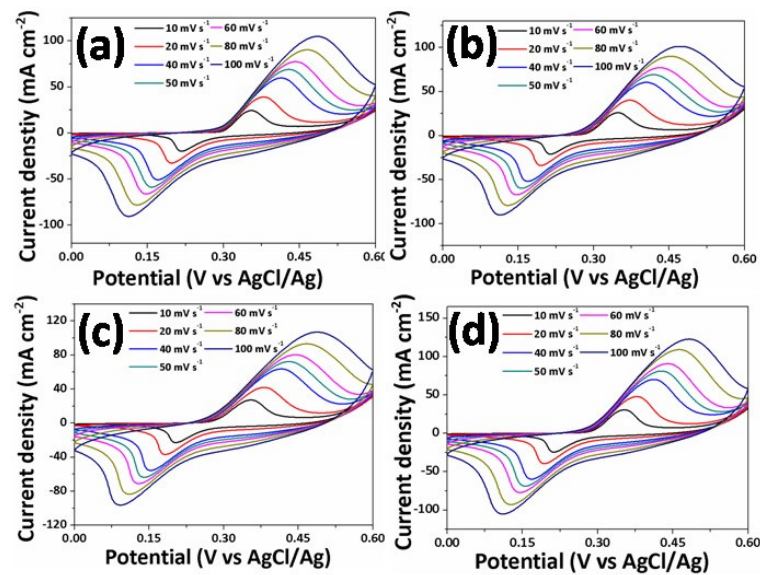


Fig. S12 CV curves of Ni-Co-S/LIG with different Co content at the scan rate of 10 mV s^{-1}

(a) 2%, (b) 6%, (c) 10%, (d) 15%

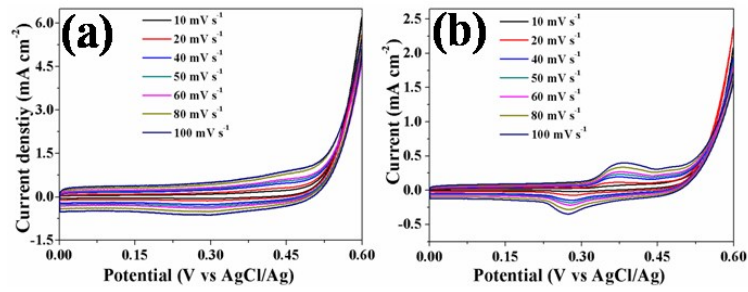


Fig. S13 CV curves of LIG (a), starch-LIG (b)

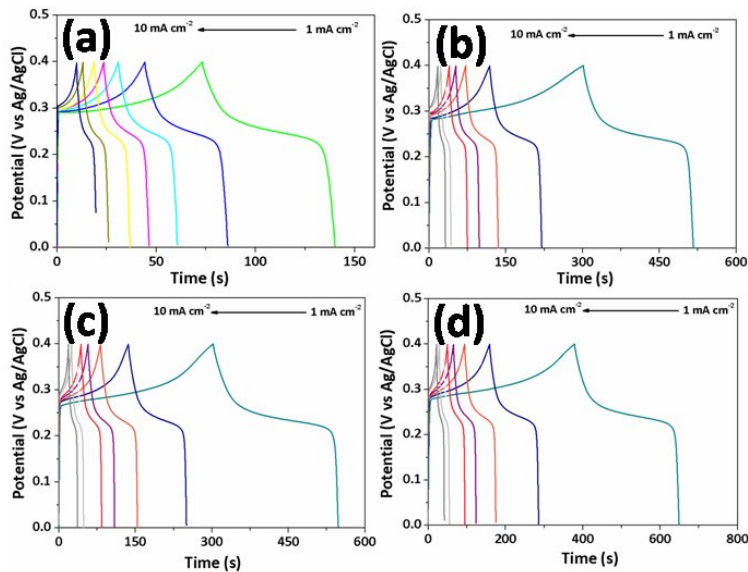


Fig. S14 GCD curves of Ni-Co-S/LIG with different Co content

(a), 0%, (b), 2%, (c), 6%, (d) 10%

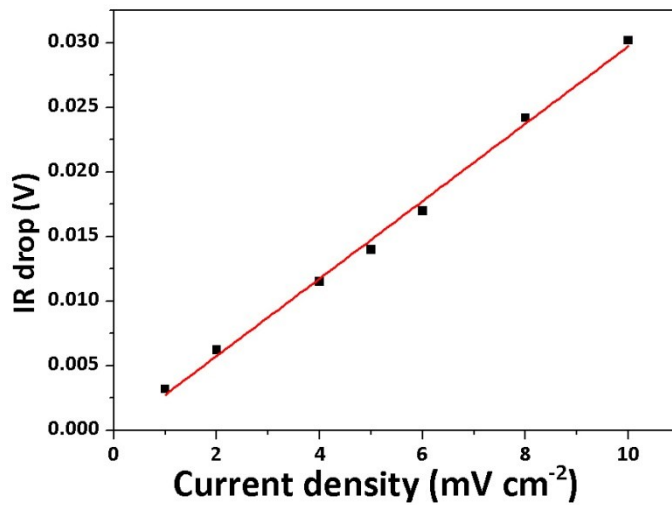


Fig. S15 IR drop of Ni-Co-S/LIG (Co-15%)//AC at different discharge current densities

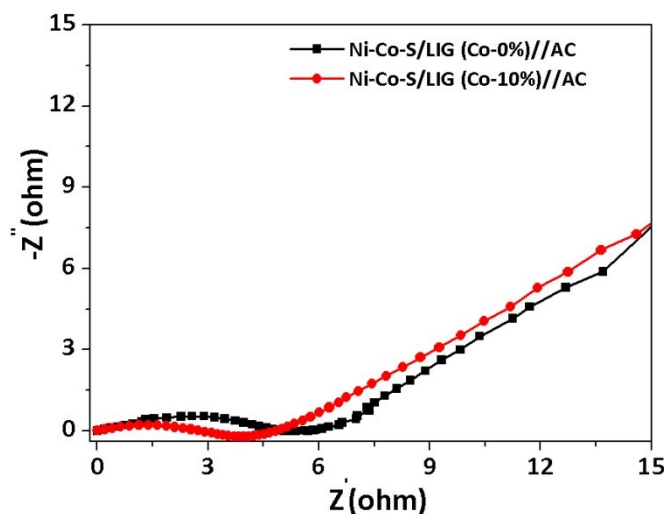


Fig. S16 Nyquist plot of the ASC device (Co-10%)

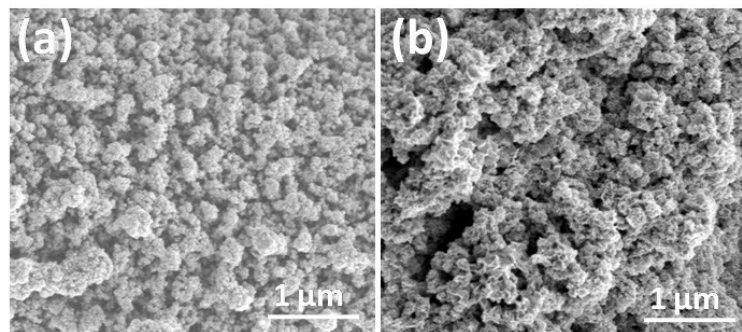


Fig. S17 SEM images of Ni-Co-S/LIG (Co-15%) before (a) and after (b) 8000 cycles

Table S3 Comparison of the maximum energy densities, corresponding average power density based on active materials and potential window of some reported nickel or cobalt sulfide based asymmetric supercapacitors

Positive materials//negative materials	electrolyte	Areal Capacitance (mF/cm ²)	Energy density (μWh cm ⁻²)	Power density (μW cm ⁻²)	Ref.
LIG-MnO ₂ -MSCs	LiCl/PVA	934	32.4	2334	S1
LIG-PANI-MSCs	PVA/H ₂ SO ₄	361	8.0	649	S1
LIG-FeOOH//LIG- MnO ₂	PVA/H ₂ SO ₄	21.9	9.6	11853	S1
MnO ₂ /CNT/nylon FSCs	PVA/ LiCl	40.9	2.6	66.9	S2
LIG	LiCl/PVA	0.8	0.03	2290	S1
GQDs//MnO ₂	0.5 M Na ₂ SO ₄	1.107	0.154	7.51	S3
GF@3D-Gs FSCs	PVA/H ₂ SO ₄	1.7	0.17	6	S4

MnO ₂	-	56.3	5.01	12020	S5
SWCNTs/PANI NWs yarn-based SCs	PVA/H ₂ SO ₄	6.23	0.1	148	S6
NiO	1M KOH	1.24	1.0	40000	S7
LIG-MoS ₂	NaCl/PVP	14	2.8	440	S8
MWCNT/OMC FSCs	PVA/H ₂ SO ₄	39.7	1.77	43	S9
PANI-SS FSCs	PVA/H ₂ SO ₄	19	0.95	100	S10
LIG-O ₂	PVA/H ₂ SO ₄	37	0.48	120	S11
Ni-Co-S/LIG//AC	2M KOH	160	56.9	8000	This work

[S1] L. Li, J. Zhang, Z. Peng, Y. Li, C.Gao, Y. Ji, et al, *Advanced Materials*, 2016, 28, 838-845.

[S2] C. Choi, S.-H. Kim, H. J. Sim, J. A. Lee, A. Y. Choi, Y. T. Kim, et al, *Sci. Rep.*, 2015, 5, 9387-9393.

[S3]. W. W. Liu, Y. Q. Feng, X. B. Yan, J. T. Chen, Q. J. Xue, *Adv. Funct. Mater.*, 2013, 23, 4111-4122.

[S4] Y. Meng, Y. Zhao, C. Hu, H. Cheng, Y. Hu, Z. Zhang, G. Shi, L. Qu, *Adv. Mater.*, 2013, 25, 2326-2331.

[S5] X. Wang, B. D. Myers, J. Yan, G. Shekhawat, V. Dravid, P. S. Lee, *Nanoscale* 2013, 5, 4119-4122.

[S6] Q. Meng, K. Wang, W. Guo, J. Fang, Z. Wei, X. She, *Small*, 2014, 10, 3187-3193.

[S7] E. Eustache, R. Frappier, R. L. Porto, S. Bouhtiyya, J. F. Pierson, T. Brousse, *Electrochem. Commun.*, 2013, 28, 104-106.

[S8] F. Claerici, M. Fontana, S. Bianco, M. Serrapede, F. Perrucci, S. Ferrero, et al, *ACS Appl. Mater. Interfaces*, 2016, 8, 10459-15465.

[S9] J. Ren, W. Bai, G. Guan, Y. Zhang, H. Peng, *Adv. Mater.*, 2013, 25, 5965-5970.

[S10] Y. Fu, H. Wu, S. Ye, X. Cai, X. Yu, S. Hou, H. Kafafy, D. Zou, Integrated power fiber for energy conversion and storage. *Energy Environ. Sci.* 6 (2013) 805-812.

[S11] Y. Li, D. X. Luong, J. Zhang, Y. R. Tarkunde, C. Kittrrell, F. Sargunaraj, et al, Laser-Induced Graphene in Controlled Atmospheres: From Superhydrophilic to Superhydrophobic Surfaces. *Adv. Mater.* 29 (2017) 1700496.

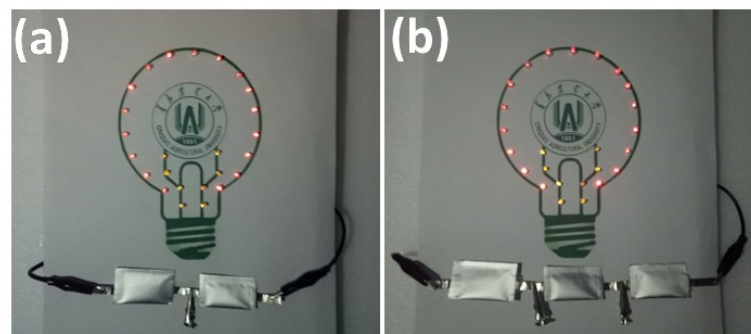


Fig. S18 The photograph of 25 commercial red LEDs powered by two (a) and three (b) Ni-Co-S/LIG//AC asymmetric MSCs in series